Time-Resolved Phase Measurement of a Self-Amplified Free-Electron Laser

Yuelin Li, John Lewellen, Zhirong Huang, Vadim Sajaev, and Stephen V. Milton
Advanced Photon Source, Argonne National Laboratory, Argonne, Illinois 60439
(Received 27 August 2002; published 18 November 2002)

We report on the first time-resolved phase measurement on self-amplified spontaneous emission (SASE) free-electron laser (FEL) pulses. We observed that the spikes in the output of such free-electron laser pulses have an intrinsic positive chirp. We also observed that the energy chirp in the electron bunch mapped directly into the FEL output. Under certain conditions, the two chirps cancel each other. The experimental result was compared with simulations and interpreted with SASE theory.

DOI: 10.1103/PhysRevLett.89.234801 PACS numbers: 41.60.Cr, 42.25.Bs, 42.55.Vc, 52.59.Rz

Single-pass, high-grain free-electron lasers (FELs) based on self-amplified spontaneous emission (SASE) [1,2] are proposed for the next generation of high-brightness, coherent x-ray sources with ultrashort pulse durations [3,4]. Recent experiments have demonstrated saturation of such SASE FELs [5–7] and its capability of achieving shorter and tunable wavelengths by direct amplification [6] as well as harmonic generations [7,8].

In a SASE FEL, a favorable instability occurs due to the interaction of an electron beam and the electromagnetic wave it produces as the beam propagates down an undulator. Provided the interaction is strong enough, the radiation power grows exponentially with the undulator distance until it reaches saturation [1,2]. In general, a SASE FEL has excellent transverse coherence because a single transverse mode with the largest gain dominates. However, a SASE pulse has poor temporal coherence and complicated temporal structure since the process is initiated by shot noise in the electron beam. In this Letter, we report to our knowledge the first single-shot time-resolved characterization of SASE pulses. The measurement reveals both amplitude and phase of the radiation using the frequency-resolved optical gating (FROG) technique [9]. Such information is essential for any future x-ray FEL and critical for many schemes proposed to tailor the SASE temporal profiles, such as chirped pulse [10] slicing and compression.

The measurement was conducted at the Low-Energy Undulator Test Line at the Advanced Photon Source. A detailed description of the facility was presented earlier [5,11]. Table I is a summary of the main parameters for this experiment. Briefly, a high-brightness electron bunch generated from an rf photocathode gun is compressed through a magnetic chicane and then accelerated to 217 MeV in energy and sent into an undulator line. The adjacent 2.4-m-long undulators are separated by 38 cm for phase matching between them. This gap also allows room for electron beam and optical diagnostics, and control magnets. Details of the electron beam and optical diagnostics suite can be found in [11]. A mirror at each station can also direct the SASE light toward diagnostics located outside of the tunnel.

Only the first five of the eight undulators are used in this experiment. A negative chirp of the electron bunch $\sigma_\delta/\sigma_z \approx -25\ \mathrm{m}^{-1}$ is determined by measuring the energy spread on a spectrometer using a modified linac zero-phasing technique. Here σ_δ is the relative correlated energy spread, and σ_z is the rms bunch length. Exponential gain and saturation was verified, and a gain length of $L_G = 0.68$ m was measured (Fig. 1). The SASE output from undulator 5 is directed through a number of collimating optics with a total of 1.9 cm of fused silica to a single-shot FROG device using the second harmonic gating geometry [9] and an energy meter.

The FROG device records single-shot spectrograms of the second harmonic correlation signal of two replicas of the input pulses from a 0.5-mm type I β-barium borate crystal. In this setup, the autocorrelation field signal is $E_{\mathrm{sig}}(t,\tau) \propto E(t)E(t-\tau)$, where τ is the relative delay. When recording the spectrum, the observed trace is the so-called spectrogram, $I_{\mathrm{FROG}}(\omega,\tau) \propto |\int_{-\infty}^{\infty} E_{\mathrm{sig}}(t,\tau) \times \exp(-i\omega t)dt|^2$, and contains both amplitude and phase of the input, which is then retrieved using an iterative algorithm. Note that, for this FROG geometry, there is an ambiguity about the direction of time.

TABLE I. Main experimental parameters.

Beam energy (γmc^2)	217 MeV
Bunch charge	1 nC
rms bunch length (σ_z)	0.5 ps
Peak current	0.85 kA
rms uncorrelated energy spread ($\sigma_\delta^{\mathrm{inc}}$)	0.3%
rms correlated energy spread (σ_δ)	0.4%
Bunch chirp (σ_δ/σ_z)	−25 per meter
rms normalized emittance	9π mm mrad
Undulator period (λ_u)	3.3 cm
Undulator peak field	1 T
Undulator length (each)	2.4 m
Undulator strength parameter (K)	3.1
Nominal radiation wavelength (λ)	530 nm
Measured gain length (L_g)	0.68 m
Energy per pulse (W)	60 μJ

 0031-9007/02/89(23)/234801(4)$20.00

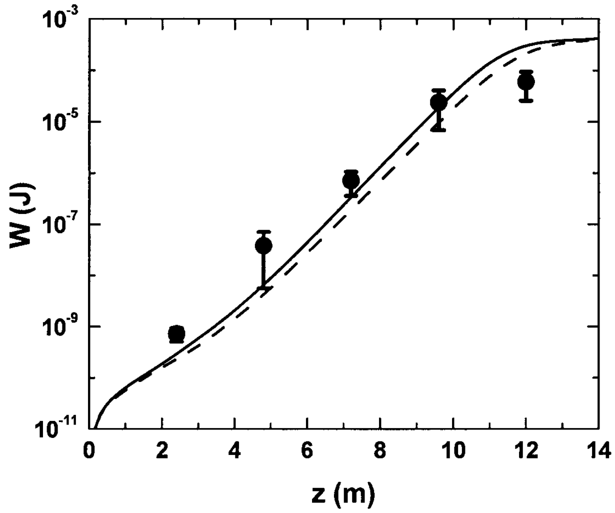

FIG. 1. SASE output energy versus distance. Data points are experimental measurement and the lines are from GINGER simulations using the conditions listed in Table I with an electron bunch chirp (dashed line) and without the chirp (solid line). The measured gain length is 0.68 m. There is no normalization between the experimental and simulation data.

Example traces of the FROG measurement along with the retrieved pulse shape, phase, and instantaneous frequency in the time domain are given in Figs. 2(a) and 2(b). Note that the instantaneous frequency is obtained by differentiating the phase; hence, spikes caused by phase discontinuity should be disregarded. The reconstructed traces closely follow the measured traces though the raw traces are dramatically different from each other.

Figure 2(a) depicts a single spike-dominated trace with FWHM pulse duration and bandwidth of 175 fs and 2.9 nm, respectively. We notice the asymmetry in the frequency direction with both ends of the trace pointing towards higher frequency. This indicates that there is more than one spike in the field and there is a frequency shift between them. The retrieval in the time domain reveals a second small pulse, which has a frequency shift of about 2% with respect to the main spike, while the frequency shift within the main spike is a factor of 3 smaller.

For the trace with multiple spikes in Fig. 2(b), the asymmetry in the frequency axis is again visible, with more significant frequency shift during the spikes and abrupt frequency change at the edges of the spikes. For both cases, there are clearly phase discontinuities at the edge of some spikes.

To interpret the observation in Fig. 2, we recall that the temporal characteristics of a SASE pulse are those of chaotic light due to the noisy start-up. Under the one-dimensional, cold beam approximation, the electric field in the exponential growth regime is a sum of N_e wave packets [12,13]

$$E(t, z) = E_0(z) \sum_{j=i}^{N_e} \exp\left[i\omega_r(t - t_j) + \frac{(t - t_j - z/v_g)^2}{4\sigma_t^2}\left(1 + \frac{i}{\sqrt{3}}\right)\right], \quad (1)$$

where N_e is the total number of electrons in the

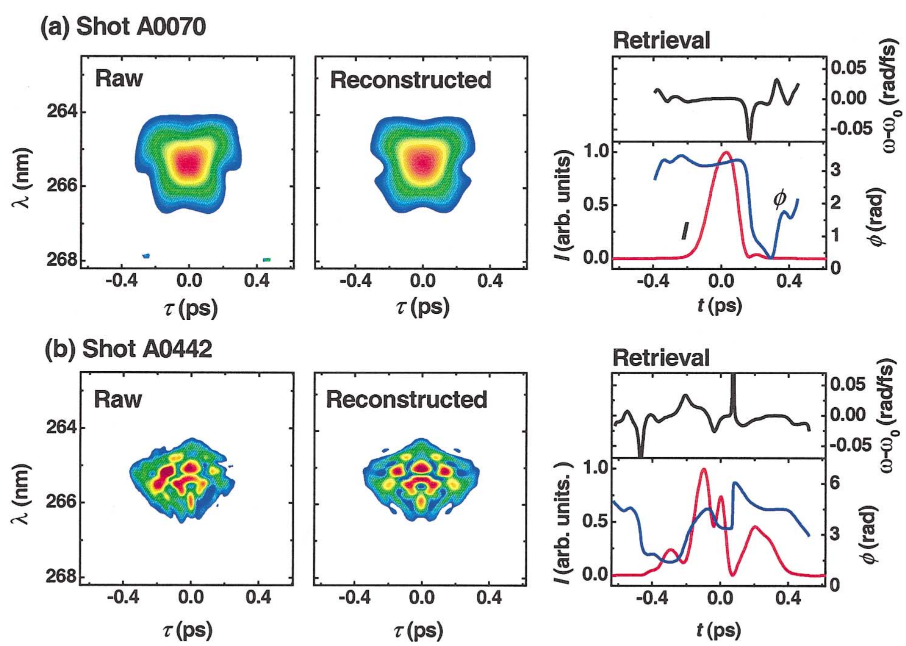

FIG. 2 (color). Example FROG traces and their retrievals showing instantaneous frequency (black), the phase (blue), and intensity (red) as a function of time. (a) A single-spike dominated case and (b) a multiple-spike case. Note that both raw traces show a symmetric pattern in the time direction with unbalanced intensity. The sharp spikes in the frequency plots are due to the phase discontinuity. The retrievals are shown in the correct time direction.

bunch, $E_0(z)$ contains the exponential growing factor,

$$\omega_r = \frac{4\pi c \gamma^2}{\lambda_u(1 + K^2/2)} \tag{2}$$

is the resonant frequency, t_j is the random arrival time of the jth electron, v_g is the group velocity of each wave packet with the rms coherence length $\sigma_t \approx (N_u/\rho)^{1/2}/2\omega_r$, N_u is the number of undulator periods, and ρ is the FEL scaling parameter [2]. Analysis shows that, for an electron bunch with an FWHM duration T, the SASE pulse is organized into $M \approx T/4\sigma_t$ coherent spikes separated roughly by $4\sigma_t$ [13]. The phase of the electric field is correlated within a coherent spike but is uncorrelated between spikes. Moreover, due to the requirement of phase matching between the SASE pulse and the electrons, v_g is slightly less than the speed of light in a vacuum [12], and an intrinsic chirp exists within a coherent spike as indicated by the quadratic phase term of $(t - t_i - z/v_g)^2/4\sqrt{3}\sigma_t^2$ in Eq. (1). For a chirped electron bunch, the gain length is slightly increased as compared to the unchirped case [14], and the radiation field becomes

$$E(t, z) = E_0(z)\sum_{j=i}^{N_e}\exp\bigg[i[\omega_0 + \Phi''_\gamma(t - t_0)](t - t_j) + \frac{(t - t_j - z/v_g)^2}{4\sigma_t^2}\bigg(1 + \frac{i}{\sqrt{3}}\bigg)\bigg], \tag{3}$$

where $\Phi''_\gamma = \omega_0 c \sigma_\delta/\sigma_z$ is the effect of the electron beam energy chirp with ω_0 being the central frequency at t_0. Because of the electron chirp and the resonant condition [i.e., Eq. (2)], an overall frequency chirp exists from spike to spike through Φ''_γ. Collecting all coefficients of quadratic terms in Eq. (3), the complex pulse form factor is

$$\Gamma_0 = \Phi''_\gamma + \frac{1}{4\sigma_t^2}\bigg(\frac{1}{\sqrt{3}} - i\bigg).$$

To analyze the experimental data, we take into account the pulse propagation effect in the collecting optics and determine the final pulse form factor using $1/\Gamma = 1/\Gamma_0 - i\Phi''_m$ [15]. Here $\Phi''_m = 2\beta'' L_m$ with a group velocity dispersion $\beta'' = 660$ fs^2/cm and a thickness $L_m = 1.9$ cm of fused silica in the collecting optics, respectively. The final chirp for the detected signal is

$$\phi'' = \frac{d^2\phi}{dt^2} = 2\mathrm{Im}(\Gamma) = 2\frac{\Omega\Theta + \Phi''_m}{\Omega^2 + \Phi''^2_m}, \tag{4}$$

where $\Omega = 4\sigma_t^2 - \Phi''_m\Theta$, $\Theta = 1/\sqrt{3} + 4\sigma_t^2\Theta''_\gamma$.

An interesting scenario for Eq. (4) is when the electron bunch chirp and the intrinsic SASE chirp have opposite signs and $\Theta = 1/\sqrt{3} + 4\sigma_t^2\Phi''_\gamma \approx 0$. In this case, the two chirps cancel each other and a transform-limited pulse can be obtained at the SASE output. At the detector we have $\phi'' = 2\Phi''_m/(16\sigma_t^4 + \Phi''^2_m) \sim \Phi''_m/8\sigma_t^4$ if Φ''_m is small enough. This is actually the case for the shot in Fig. 2(a). Approximating the pulse shape as Gaussian, we can use the rms pulse duration (75 fs) as the coherence length. With an estimated electron bunch chirp of -25 m^{-1}, we have $\Theta \sim 0.03$, hence, $\phi'' \sim 8$ μrad/fs^2, while the FROG retrieval gives $|\phi''| \approx 12$ μrad/fs^2.

A more quantitative analysis is illustrated in Fig. 3, which depicts the experimentally measured chirp $|\phi''|$ as a function of the coherence length. In the data analysis, only well-isolated spikes with no visible intraspikes are used. Again, the spike shape is assumed to be Gaussian, and the rms pulse duration is used for the coherence length. Because of the intrinsic jitter and complicated behavior of each spike, the data are rather scattered. Even so, one can clearly identify a sharp dip at around $\sigma_t = 75$ fs, which corresponds to $\Theta \approx 0$. By slightly adjusting the electron bunch chirp in Eq. (4), we are able to fit the position of the dip at about -28 m^{-1} (see curves in Fig. 3).

Figures 2 and 3 unambiguously reveal the positive intrinsic SASE chirp, confirming the theoretical prediction in Eq. (1). They also verify that the electron beam energy chirp directly maps into the FEL output, a key process for compressing and slicing the pulse from future x-ray FELs. Figure 3 also serves as an independent measurement of the electron bunch energy chirp.

The dip in Fig. 3 also divides spike properties into two regimes. When $\Theta > 0$, i.e., $4\sigma_t^2\Phi''_\gamma > -1/\sqrt{3}$, which is the long pulse regime, we eventually have $\phi'' \approx 2\Phi''_\gamma$ at very long coherence length. For the SASE FEL, this normally does not happen, as coherence length is limited both by gain length and the lasing wavelength.

The other regime is when $\Theta < 0$, i.e., $4\sigma_t^2\Phi''_\gamma < 1/\sqrt{3}$. In this case, the SASE intrinsic chirp can dominate and the final chirp is $\phi'' \approx 1/4\sqrt{3}\sigma_t^2$ as the coherence length becomes short enough. Clearly, this is more the case for

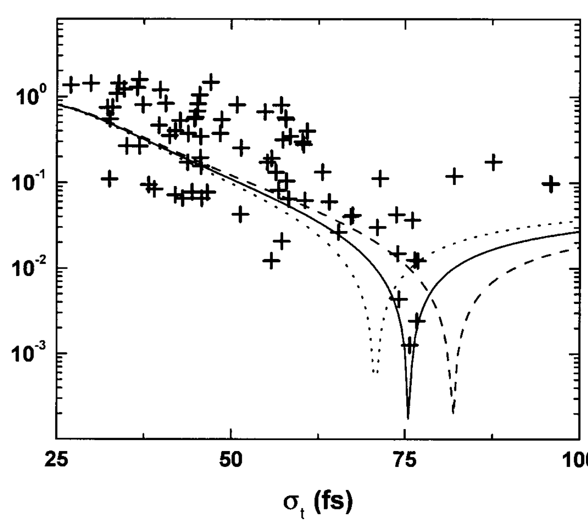

FIG. 3. Magnitude of the chirp of the SASE spikes. The data points are experimental measurement using the FROG. The curves are fit using Eq. (4) with an electron chirp of -24 m^{-1} (dashed line), -28 m^{-1} (solid line), and -33 m^{-1} (dotted line).

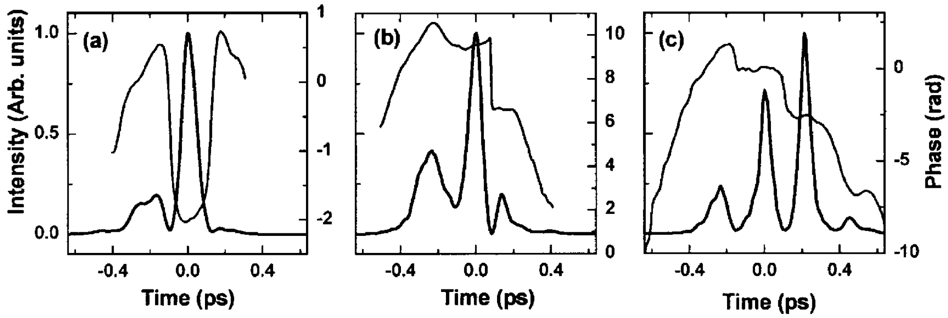

FIG. 4. GINGER simulation using the conditions listed in Table I, showing the intensity (bold lines) and phase (thin lines) as a function of time. (a) No chirp; (b) $-17\ \mathrm{m}^{-1}$ chirp, with a single dominant spike; and (c) with a $-17\ \mathrm{m}^{-1}$ chirp, showing multiple spikes. The phase during the spikes is almost flat in (b) and (c) due to the opposite sign of the SASE intrinsic chirp and the electron bunch chirp.

the data in Fig. 2(b). For future x-ray FELs, this will be the dominating regime due to the short wavelength.

In this experiment, the measured average rms coherence length, both from the FROG and the gain length data, is about 60 fs. This is why there are more data points on the shorter coherence length side in Fig. 3.

It is now straightforward to remove the ambiguity in the time direction of the FROG measurement. First, with short enough spikes, the parabolic phase shape is a direct indication of the time direction. Second, with a positive chirp during the SASE spike, there should be an abrupt frequency down-shift at the end of the spike. As there is no communication between spikes, this should also be accompanied by a phase jump of random size. Figure 2 actually displayed the correct time direction in the retrievals.

The observation is compared with GINGER [16] SASE simulations, which uses the electron condition in Table I for both unchirped and chirped beams. The chirp of the electron bunch was adjusted for generating the flat phase. The comparisons of the output energy as a function of z are shown in Fig. 1 as curves, and Figs. 4(a)–4(c) show both the intensity and the phase as a function of time for the on-axis radiation ($r = 0$).

In conclusion, we observed a positive intrinsic chirp in the SASE FEL spikes, and we confirmed that the energy chirp in the electron bunch does map to the SASE output. These observations have very important applications for future x-ray FEL sources in pulse engineering and manipulation. It is also shown that, by careful control of the electron beam parameters such as the bunch length and the energy chirp, it is possible to obtain transform-limited FEL pulses. The FROG traces also provide rich information on the statistics of the SASE output; however, this is beyond the scope of this Letter.

The authors are grateful for help by O. Markarov and R. Dejus for performing the gain length measurement and processing the data. We also thank K.-J. Kim and L. Teng for insightful discussions. This work is supported by the U.S. Department of Energy, Office of Basic Energy Sciences, under Contract No. W-31-109-ENG-38.

[1] A. M. Kondratenko and E. L. Saldin, Sov. Phys. Dokl. **24**, 986 (1979).
[2] R. Bonifacio, C. Pellegrini, and L. M. Narducci, Opt. Commun. **50**, 373 (1984).
[3] M. Cornacchia *et al.*, Stanford Linear Accelerator Center Report No. SLAC-R-521, revised 1998.
[4] DESY Report No. DESY97-048, edited by R. Brinkmann, G. Materlik, J. Rossbach, and A. Wagner, 1997.
[5] S. V. Milton *et al.*, Science **292**, 2037 (2001).
[6] V. Ayvazyan *et al.*, Phys. Rev. Lett. **88**, 104802 (2002).
[7] A. Tremaine *et al.*, Phys. Rev. Lett. **88**, 204801 (2002).
[8] S. G. Biedron *et al.*, Nucl. Instrum. Methods Phys. Res., Sect. A **483**, 94 (2002).
[9] R. Trebino *et al.*, Rev. Sci. Instrum. **68**, 3277 (1997).
[10] C. Pellegrini, Nucl. Instrum. Methods Phys. Res., Sect. A **445**, 124 (2000).
[11] E. Gluskin *et al.*, Nucl. Instrum. Methods Phys. Res., Sect. A **429**, 358 (1999).
[12] R. Bonifacio *et al.*, Phys. Rev. Lett. **73**, 70 (1994).
[13] K.-J. Kim, *Towards X-Ray Free-Electron Lasers*, edited by R. Bonifacio and W. A. Barletta (American Institute of Physics, New York, 1997), p. 3.
[14] C. B. Schroeder *et al.*, Nucl. Instrum. Methods Phys. Res., Sect. A **483**, 89 (2002).
[15] A. E. Siegman, *Lasers* (University Science Books, Sausalito, CA, 1986), p. 338.
[16] W. Fawley, Report No. LBNL-49625, 2001.